

Direct and indirect causes of Fermi level pinning at the SiO/GaAs interface

Darby L. Winn, Michael J. Hale, Tyler J. Grassman, and Andrew C. Kummel
Department of Chemistry and Biochemistry, University of California, San Diego, La Jolla, California 92093

Ravi Droopad and Matthias Passlack
Freescale Semiconductor, Inc., Tempe, Arizona 85284

(Received 14 April 2006; accepted 18 September 2006; published online 23 February 2007)

The correlation between atomic bonding sites and the electronic structure of SiO on GaAs(001)- $c(2 \times 8)/(2 \times 4)$ was investigated using scanning tunneling microscopy (STM), scanning tunneling spectroscopy (STS), and density functional theory (DFT). At low coverage, STM images reveal that SiO molecules bond Si end down; this is consistent with Si being undercoordinated and O being fully coordinated in molecular SiO. At $\sim 5\%$ ML (monolayer) coverage, multiple bonding geometries were observed. To confirm the site assignments from STM images, DFT calculations were used to estimate the total adsorption energies of the different bonding geometries as a function of SiO coverage. STS measurements indicated that SiO pins the Fermi level midgap at $\sim 5\%$ ML coverage. DFT calculations reveal that the direct causes of Fermi level pinning at the SiO GaAs(001)- (2×4) interface are a result of either local charge buildups or the generation of partially filled dangling bonds on Si atoms. © 2007 American Institute of Physics. [DOI: [10.1063/1.2363183](https://doi.org/10.1063/1.2363183)]

I. INTRODUCTION

Early attempts to fabricate a GaAs-based metal-oxide-semiconductor field-effect transistor focused on using either SiO₂ (Refs. 1–5) or the native oxide of GaAs (Refs. 6–8) as the gate dielectric. Unfortunately, both oxides were found to induce states within the band gap, pinning the Fermi level.^{9–11} The Fermi level is considered pinned when an external potential can no longer modulate the Fermi level position making a device inoperable. In the case of GaAs's native oxide, Fermi level pinning was initially attributed to excess As on the surface,^{12–16} but an atomic level understanding of the oxide/GaAs interface did not exist. Since the two conventional oxides (SiO₂ and the native oxide) pin the Fermi level, a broad search of other oxides was needed to find a gate dielectric material that would passivate the GaAs surface, leaving the Fermi level unpinned.

In an effort to find an appropriate oxide, research efforts have recently shifted to include not only macroscopic studies [capacitance voltage (CV), photoluminescence, etc.] but also microscopic studies [scanning tunneling microscopy (STM) and scanning tunneling spectroscopy (STS)]. These microscopic studies (Hale *et al.*^{17,18} and Negoro *et al.*¹⁹) have given insight into the atomic structures of adsorbates bound to the GaAs(001)- $c(2 \times 8)/(2 \times 4)$ surface and revealed that the cause of the Fermi level pinning was not excess As on the surface.

Several macroscopic studies have been performed on the SiO/GaAs interface,^{20–23} but none on the atomic level. Building on previous work, the results presented in this manuscript show how the exact atomic placement of SiO adsorbates influences the electronic structure of SiO/GaAs(001)- $c(2 \times 8)/(2 \times 4)$ system.

II. EXPERIMENTAL TECHNIQUE

Experiments were performed in an UHV chamber with a base pressure of 3×10^{-10} Torr. The chamber is equipped with low energy electron diffraction (LEED) and a Park Scientific AutoProbe VP STM with STS capabilities. As₂-capped (~ 25 nm) *n*- and *p*-type molecular beam epitaxially grown GaAs samples were used for the study, with Si and Be dopant concentrations of 2×10^{17} cm⁻³, respectively. Both *n*- and *p*-type samples appear identical in STM images but differ in electronic properties.

To prepare the samples for STM, a thermal decapping procedure was employed. Initially, the samples were degassed at 200 °C for at least 2 h to remove the weakly bound adsorbates such as water. This was followed by 10–50 cycles of 2 min temperature ramps to 420 °C followed by instantaneous drops in temperature and stabilization at 50 °C for another 2 min to remove the As₂ cap. These cycles were repeated until there was no pressure rise due to As desorbing from the surface. A plot of the temperature ramps and subsequent pressure rises can be found on EPAPS.²⁴ Following the decapping procedure, the surface order was verified by both LEED and STM. Variable tip-sample separation STS (dI/dV) measurements were taken utilizing an ac modulated input signal and a lock-in amplifier.^{25–27} STS was used to confirm that the clean surface was unpinned.

Once the atomic and electronic structures of the clean GaAs(001)- $c(2 \times 8)/(2 \times 4)$ surface were characterized, the samples were dosed with molecular SiO. The SiO was deposited from sintered SiO powder heated to 950 °C in a differentially pumped effusion cell. SiO powder has been shown to evaporate congruently as molecular SiO with no other oxide species, at low evaporation temperature and pressure,^{27–29} similar to our operating conditions. The depo-

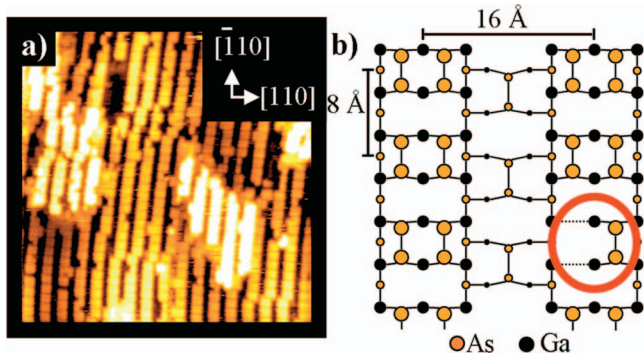


FIG. 1. (Color) (a) $300 \times 300 \text{ \AA}^2$ filled-state STM image ($V_s = -3 \text{ V}$, $I_t = 0.2 \text{ nA}$) of a clean GaAs(001)- $c(2 \times 8)/(2 \times 4)$ surface. (b) Ball-and-stick diagram showing the atomic positions of the GaAs(001)- $c(2 \times 8)/(2 \times 4)$ surface reconstruction with one of the most common defects, a missing As dimer, circled in red.

sition was performed at a main chamber pressure of $\sim 2 \times 10^{-8}$ Torr with the sample held at $\sim 14^\circ \text{C}$; postdeposition anneals were found to have no influence on the bonding geometries. After SiO deposition, STM and STS measurements were again used to characterize the surface.

III. EXPERIMENTAL RESULTS AND DISCUSSION

A. Scanning tunneling microscopy images and line scans

Figure 1(a) is a filled-state STM image of the clean GaAs(001)- $c(2 \times 8)/(2 \times 4)$ surface. The bright rows that run in the $[\bar{1}10]$ direction are comprised of first-layer electronegative As dimer pairs.^{28–34} A ball-and-stick diagram of the GaAs(001)- (2×4) surface is provided in Fig. 1(b). The As dimers that reside in the troughs are not resolved with these imaging conditions due to tunneling between the trough edge atoms and the tip, prohibiting the tip from fully entering the trough.³⁵

The actual GaAs(001) surface structure is a mixture of the $c(2 \times 8)$ and (2×4) surface reconstructions.^{29,35} The difference between the two reconstructions is subtle: in the $c(2 \times 8)$ surface structure, consecutive As dimer rows are staggered by $\frac{1}{2}$ of a unit cell along the $[\bar{1}10]$ direction, instead of lining up across the trough, as seen in the (2×4) reconstruction. However, both structures have the same electronic properties and few defects ($< 2\%$). The two most common imperfections (missing As dimers and excess As) observed via STM are a result of the thermal decapping procedure. Missing As dimers result from the surface getting slightly too warm and are depicted in the ball-and-stick diagram in Fig. 1(b). Excess As is the most common imperfection and occurs from the nonuniform heating of the sample and is imaged as bright patches on the dimer rows.

Once the clean surface has been confirmed using LEED and STM, SiO is deposited. Figure 2(a) shows a large-scale image of the GaAs surface after depositing SiO for 1 min on room-temperature GaAs(001)- $c(2 \times 8)/(2 \times 4)$, resulting in $\sim 5\%$ ML coverage. The bright patches on the rows and troughs are the SiO bonding sites, some of which have been encircled in black. SiO is not confused with excess As because the latter generally forms clumps which span several

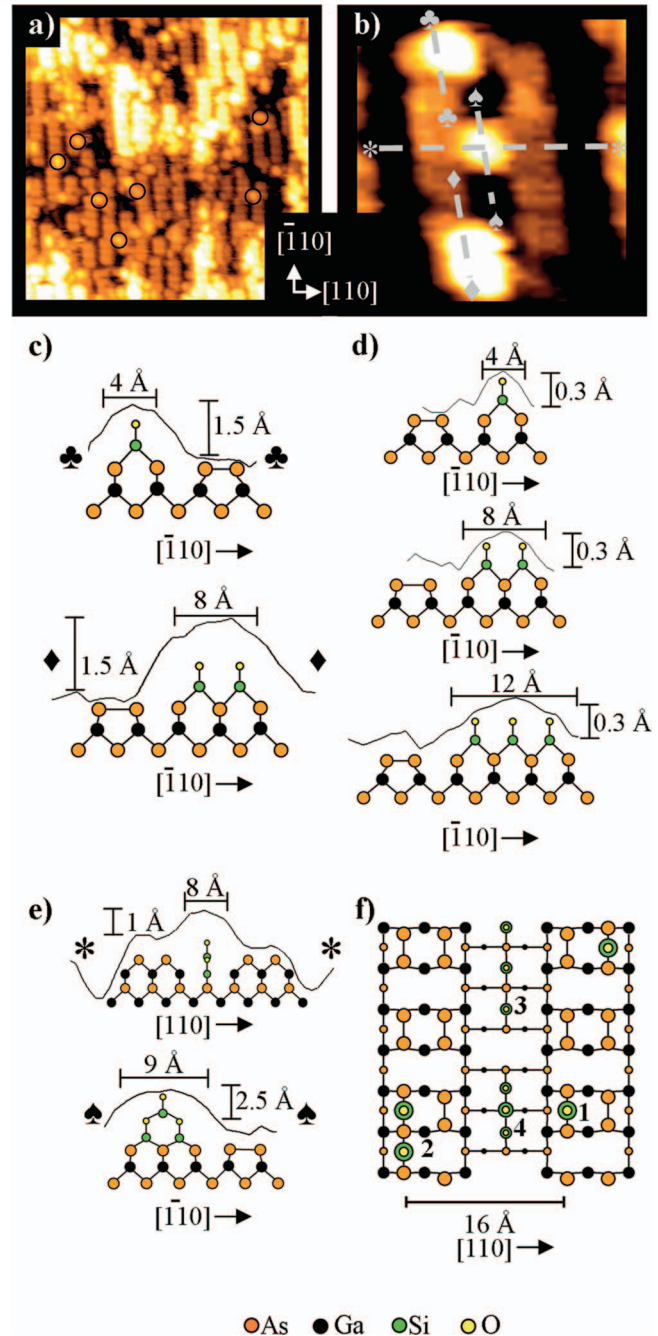


FIG. 2. (Color) (a) $300 \times 300 \text{ \AA}^2$ filled-state STM image ($V_s = -3 \text{ V}$, $I_t = 0.2 \text{ nA}$) of the GaAs(001)- $c(2 \times 8)/(2 \times 4)$ surface with $\sim 5\%$ ML coverage of SiO. Some of the SiO bonding sites have been circled in black. (b) $50 \times 50 \text{ \AA}^2$ filled-state STM image ($V_s = -3 \text{ V}$, $I_t = 0.2 \text{ nA}$) of row single, row compact double, and trough pyramid sites. (c) Line scans and ball-and-stick diagrams of the two row sites: the single (top) and compact double (bottom) sites. (d) Line scans and ball-and-stick diagrams of the trough sites that are differentiated using line scan analysis: the single (top), compact double (middle), and triple (bottom) sites. (e) Line scans and ball-and-stick diagrams of the trough pyramid site perpendicular, $[110]$ (top), and parallel, $[\bar{1}10]$ (bottom), to the trough. (f) Top-down ball-and-stick diagram of some of the most commonly observed SiO adsorption sites; the sites are labeled as indicated, “1” a row single site, “2” a row compact double site, “3” a trough triple site, and “4” a trough pyramid site.

rows. A magnified STM image showing three different SiO bonding sites is presented in Fig. 2(b); line scan analysis was performed on the STM image to help deduce the bonding sites. Figure 2(c) (top) is a line scan of the adsorption site

(bright patch) in the upper left hand corner of Fig. 2(b): this site images 4 Å long and 1.5 Å tall. It is proposed that this site consists of one SiO molecule inserting into an As dimer, denoted as a “single site.” A side-on model of the proposed row single site is shown under the line scan in Fig. 2(c) (top) and a top-down view is seen in Fig. 2(f) (site 1). The other experimentally observed row site is seen in the bottom center of Fig. 2(b). Line scan analysis [Fig. 2(c) (bottom)] reveals that this site measures twice as long in the $[\bar{1}10]$ direction as the single site and is of the same height. This site is proposed to be a “compact double site,” which consists of a SiO molecule inserting into an As dimer and an additional SiO molecule inserting between the insertion dimer and an adjacent dimer. A side-on model of the row compact double site is seen under the line scan in Fig. 2(c) (bottom) and a top-down model of the site is shown in Fig. 2(f) (site 2).

Both of the sites observed on the row are also proposed to occur in the trough region, in addition to two unique trough sites. Three of the trough sites (single, compact double, and triple sites) are not casually observed in the STM images. This is due to the lack of trough resolution at these tunneling conditions, as discussed previously. These sites, however, can be characterized by line scan analysis. Line scan analysis shows that the trough single [Fig. 2(d) (top)] and the trough compact double [Fig. 2(d) (middle)] are of the same length in the $[\bar{1}10]$ direction as the corresponding sites on the row. Side-on models of the single and compact double sites are seen under their line scans. The third type of trough site, also observed only by line scan analysis, has no row-type analogue and measures 12 Å long in the $[\bar{1}10]$ direction [Fig. 2(d) (bottom)]. This site is proposed to be two SiO molecules inserting into adjacent dimers and a third SiO molecule inserting between them; this site is denoted as a “triple site.”

Another site that is only observed in the trough is shown via a side-on model in Fig. 2(e). Unlike the trough sites in Fig. 2(d), the site in Fig. 2(e) is consistently observed in experimental STM images. This site measures ~ 1 Å higher than the row, which is too tall to be a simple insertion site (i.e., it must contain stacked SiO molecules). Although such a conclusion cannot be reached exclusively from STM images, this site is proposed to be a “pyramid site.” Other data will be presented that will further substantiate this site assignment. Side-on models along the $[110]$ and $[\bar{1}10]$ directions, along with line scans of the pyramid site, are seen in Fig. 2(e). In addition, a top-down model of the pyramid site is shown in Fig. 2(f) (site 4).

The STM images strongly suggest that SiO bonds Si end down, which is consistent with simple chemical principles. The valence shell of a Si atom contains four electrons and is sp^3 hybridized, therefore, it typically forms four bonds. An O atom contains six valence electrons and typically forms only two bonds, leaving two filled dangling bonds (i.e., two lone pair orbitals). Assuming that SiO inserts Si end down, Si can form one bond with each of the surface As atoms in the dimer and form a double bond with the O atom. This allows both the O atom and the Si atom to satisfy the requirements of the octet rule.

The 1.5 Å height difference observed by STM between the SiO molecule and the dimer row (seen in the row single and compact double sites) is also consistent with SiO inserting Si end down. The images obtained from STM are a convolution of atomic position, local density of states, and electron density. If SiO inserts Si end down, the majority of the most weakly bound electron density (i.e., closest to the Fermi level) should be concentrated in the double bond between the Si and O since the highest occupied molecular orbital is concentrated in that area. For SiO bonded Si end down, the double bond should be approximately 1.5 Å above the As dimer row, which is in agreement with the experimental observations. Furthermore, the electron density in the filled dangling bonds of the O atoms have an energy level far below the Fermi level, prohibiting electrons from tunneling out of those orbitals and into the tip.^{18,36,37} If SiO were to insert O end down, the majority of the electron density near the Fermi level would be concentrated in the nonbonding orbitals of Si. This would result in a taller site than is experimentally observed.

The trough sites (single, compact double, triple, and pyramid sites) are expected to image at two different heights. In structural models, the trough is ~ 3 Å deep. However, experimentally the average trough depth is ~ 1.5 Å; therefore, anything below this height will not be directly observed. Since the trough single, compact double, and triple sites are only expected to image at ~ 1.5 Å from the bottom of the trough, one would not expect these sites to have prominent features in STM images, which is consistent with the STM data shown in Fig. 2(d). In contrast, the top double bond in the trough pyramid site is located ~ 3 Å from the bottom of the trough; therefore, one might expect the trough pyramid site to image level with the row (since the trough is ~ 3 Å deep). Experimentally the trough pyramid site is found to image ~ 1 Å above the row, slightly higher than one might predict. The height difference between the predicted and actual image height is attributed to the top O atom having a greater density of states at an energy closer to the Fermi level than a typical surface O atom (as will be discussed later in the paper). Therefore, unlike most surface O atoms, the top O atom in the trough pyramid site is imaged, resulting in the trough pyramid site imaging ~ 1 Å above the row.

B. Scanning tunneling spectroscopy

In addition to the STM images of the various SiO adsorption sites, STS (surface electronic structure) measurements were also taken using the variable tip-sample separation method developed by Feenstra and co-workers.^{25–27} With this technique, GaAs(001) was found to have a band gap of 1.4 V. Figure 3(a) presents $(dI/dV)/(I/V)$ vs V spectra [which are proportional to the density of states (DOS)] for clean n - and p -type GaAs(001)- $c(2 \times 8)/(2 \times 4)$ surfaces, respectively. The Fermi level for all given $(dI/dV)/(I/V)$ curves resides at 0 V. From the data, it can be seen that the Fermi level for n -type GaAs(001)- $c(2 \times 8)/(2 \times 4)$ resides near the conduction band and the Fermi level for p -type GaAs(001)- $c(2 \times 8)/(2 \times 4)$ resides near the valence band, as expected.

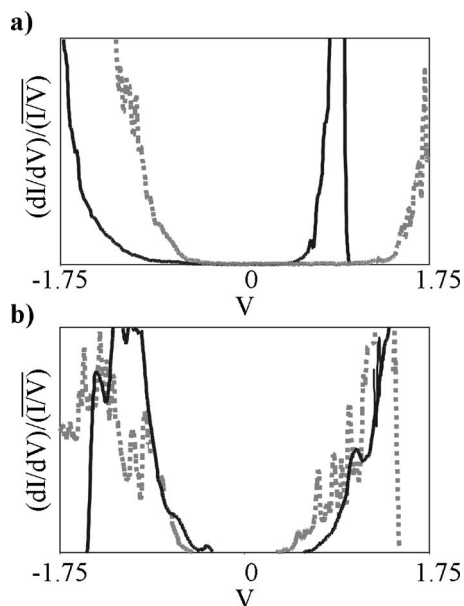


FIG. 3. STS measurements of (a) clean *n*-type (thick solid line) and *p*-type (grey dashed line) GaAs(001)- $c(2 \times 8)/(2 \times 4)$, and (b) $\sim 5\%$ ML coverage of SiO on *n*-type (thick solid line) and *p*-type (grey dashed line) GaAs(001)- $c(2 \times 8)/(2 \times 4)$. Note that both clean *n*- and *p*-type GaAs(001)- $c(2 \times 8)/(2 \times 4)$ STS plots (a) exhibit electrically unpinned surfaces, while the SiO deposited surfaces (b) are found to be pinned.

These results are typical of unpinned *n*- and *p*-type surfaces. Figure 3(b) shows STS spectra that were taken after depositing $\sim 5\%$ ML SiO on *n*- and *p*-type GaAs(001)- $c(2 \times 8)/(2 \times 4)$, respectively. In both cases, the bands are shifted, relocating the Fermi level to mid-gap; this is consistent with a pinned surface, indicating that Fermi level pinning occurs at SiO coverages as small as $\sim 5\%$ ML.

From the ball-and-stick diagram in Fig. 2(f), it can be seen that none of the proposed sites liberate As when SiO is deposited onto the surface. Furthermore, from the STM image in Fig. 2(a), no excess As deposits are seen. Therefore, excess As is certainly not the cause of the Fermi level pinning in this case.

C. Local charge buildup model

To deduce the cause of the Fermi level pinning, a closer look is taken at the transfer of electrons during SiO bonding to the surface using simple molecular orbital models. The bonding electrons of the system are located in the tetrahedral (sp^3 hybridized) orbitals of the As and Si atoms. Prior to bonding with the surface, the Si atom in a SiO molecule has two half-filled dangling bonds. In order to calculate a minimum number of electrons in the dangling bonds of the surface As atoms, the rules of the standard electron counting model are applied. These rules state that atoms contribute the same number of electrons to surface bonds as they do in the bulk material (i.e., As gives $5/4$ of an electron to Ga in the bulk, therefore it gives $5/4$ of an electron to a bond with a surface Ga atom) and atoms bonded to like atoms each give one electron to the bond.³⁸ Therefore, since the dimer As

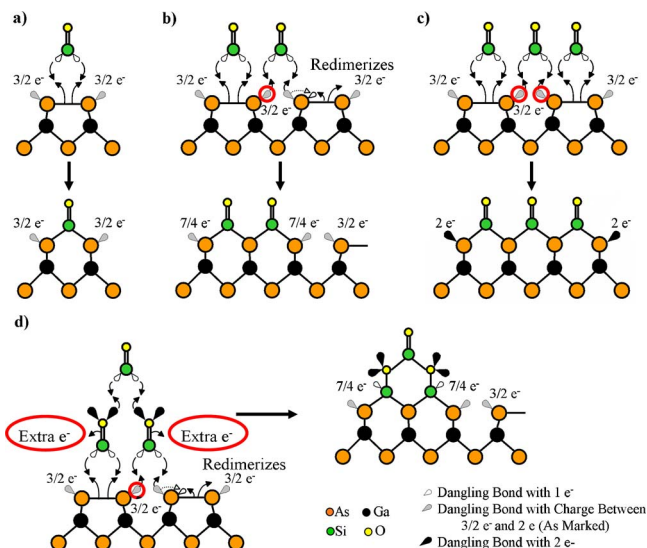


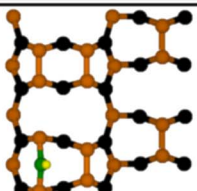
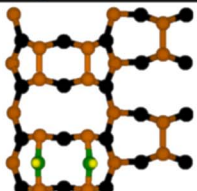
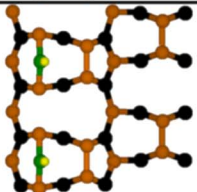
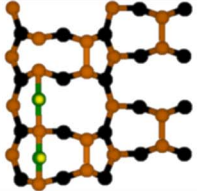
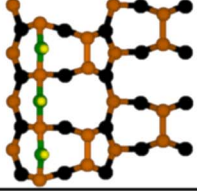
FIG. 4. Ball-and-stick diagrams of proposed SiO/GaAs(001)- (2×4) adsorption configurations before and after bonding. Arrows represent electron relocation during bonding. Prior to bonding the dangling bonds on the As atoms contain a minimum of $3/2$ electrons. The electrons noted in the dangling bonds after SiO bonding has occurred are also minimum projected values. All excess electrons caused by SiO bonding are placed in available dangling bonds. Electrons that cause a local buildup of charge are circled in red. (a) Single site, which is predicted to have no charge buildup. (b) Compact double site, which is predicted to have a small amount of charge buildup [$\sim (1/2)e^-$]. (c) Triple site, which is predicted to have a greater charge buildup than the compact double site ($1e^-$). (d) Pyramid site, which is predicted to have the same charge buildup as the compact double site but in addition causes the formation of two partially filled dangling bonds on the bottom two Si atoms.

atoms are each bonded to two Ga atoms and one As atom, the dangling bond on dimer As atoms are left with at least $3/2$ electrons.

Figure 4(a) is a ball-and-stick diagram depicting the formation of a single site, with arrows denoting the movement of electrons. In the formation of the single site, the SiO molecule inserts into the As-As bond and forms two new Si-As bonds with the surface. Each time an As-As bond is broken, each As atom gains one electron. In order to form a Si-As bond, the bond receives one electron from the dangling bond in Si and one electron from the As atom. The number of electrons needed to form the bond is exactly equal to the number of electrons available between the Si and As atoms (i.e., two electrons); therefore, no buildup of extra electrons, or local charge, on any of the atoms associated with this adsorption site is expected.

Unlike the single site, the compact double site is expected to have a small local charge buildup. The formation of the compact double site is shown in Fig. 4(b). When a compact double site forms, one SiO molecule inserts into an As dimer and the other SiO molecule inserts between that same dimer and the neighboring As dimer. The distal As atom in the neighboring dimer (that is not involved in the SiO bonding) may redimerize if the energy barrier is low enough. In the formation of the compact double site, four Si-As bonds are created. The center As atom is forced to form a total of four bonds (two Ga-As and two Si-As); therefore, the As atom can no longer have any dangling bonds. Since the pre-existing dangling bond had $3/2$ electrons, an excess of $1/2$

TABLE I. Summary of enthalpies of adsorption for row sites, with top-down models. The “ ΔH (total)” column displays the enthalpy of reaction for the entire slab. The numbers in this column are divided by the number of SiO molecules per slab and the results are displayed in the “ ΔH (per SiO)” column. It is necessary to calculate the “Corrected (per SiO)” values for structures that have an undimerized surface As atom in them. To calculate these corrected values, half of the stabilization energy for an As dimer is added to the ΔH (total) value and the resulting number is then divided by the number of SiO molecules in the slab.

Row Sites	Top Down Cut Away View	ΔH_{ads} (Total)	ΔH_{ads} (Per SiO)	Corrected (Per SiO)
Single		-1.08 eV	-1.08 eV	N/A
Horizontal Double		-2.02 eV	-1.01 eV	N/A
Vertical Double		-2.10 eV	-1.05 eV	N/A
Compact Double		-1.15 eV	-0.58 eV	-0.87 eV
Triple		-1.28 eV	-0.43 eV	N/A

● As ● Ga ● Si ● O

of an electron remains after the formation of the Si–As bonds. This excess 1/2 of an electron may then be incorporated into the local bond network and/or the partially filled dangling bonds on the outer As atoms, potentially giving the dangling bonds a minimum charge of 7/4 electrons, as seen in Fig. 4(b).

The triple and pyramid sites are expected to have larger local charge buildup, as depicted in Figs. 4(c) and 4(d), respectively. In the case of the triple site, three SiO molecules form six Si–As bonds with the surface [Fig. 4(c)]. Since the center two As atoms can no longer have dangling bonds, there remains an excess charge of one electron that must be

incorporated into the local system, which can result in the outer As atoms’ dangling bonds possessing a minimum of two electrons each. This local charge buildup should be large enough to perturb the local electronic structure and potentially pin the Fermi level.

The pyramid site is the most complicated SiO adsorption site. From Fig. 4(c), it can be seen that there are two major sources of charge buildup. The first source is the center As atom that forms two Si–As and two Ga–As bonds, similar to the compact double site. This generates an excess of 1/2 electron that needs to be incorporated into the local system (i.e., bond network and/or outer As atoms’ dangling bonds).

The second source of charge buildup occurs as a result of the undercoordination of the bottom Si atoms. In the SiO pyramid, the bottom O atoms are single bonded to two different Si atoms (as opposed to being double bonded to a single Si atom as in all of the other adsorption geometries). Therefore, the bottom Si atoms are sp^3 hybridized while all of the other Si atoms are sp^2 hybridized. Since the bottom Si atoms form three fully formed bonds (one Si–O and two Si–As) they have an additional half-filled dangling bond. These half-filled dangling bonds are predicted to generate a state in the band gap region, thereby pinning the surface.

This simple model implies that there may be two distinct direct causes of Fermi level pinning in the SiO/GaAs(001)- $c(2 \times 8)/(2 \times 4)$ system: the buildup of local charge (triple site) and partially filled dangling bonds on Si atoms (pyramid site). The validity of the local charge buildup model is further examined with DOS, projected density of states (PDOS), and atomic charge analysis from density functional theory (DFT) calculations.

IV. COMPUTATIONAL RESULTS AND DISCUSSION

A. Enthalpies of adsorption

Plane-wave (periodic boundary) DFT calculations were performed with the Vienna *ab initio* simulation package (VASP) code.^{39–42} The surface of interest was modeled using an eight layer GaAs(001) H-terminated slab with the (2×4) surface reconstruction. The bottom four layers of the slab were frozen to help simulate bulk properties. The calculations were performed using the Perdew-Burke-Ernzerhof⁴³ (PBE) variant of the general gradient approximation. Projector augmented wave (PAW) potentials were used to represent the atoms (as supplied with VASP).^{44,45} The plane wave cutoff energy was set to 400 eV, and the k -point sampling utilized was a $4 \times 4 \times 1$ Monkhorst-Pack⁴⁶ k -point sampling scheme resulting in a total of four irreducible k points in the first Brillouin zone. The structures were considered adequately relaxed once the interatomic forces were below 0.01 eV/Å.

The errors associated with these calculations are not straightforward to estimate. There are two types of errors that arise in DFT calculations: convergence errors and method errors. Convergence errors include both errors related to the choice of convergence parameters (plane-wave cutoff, k points, slab thickness, vacuum thickness, etc.) as well as relaxation parameters (maximum allowed forces on atoms). If the appropriate computational parameters are chosen, the convergence errors should be negligible compared to the method errors. The method errors encompass the errors inherent to the chosen computational method (exchange correlation functional, various approximations, atomic potential, etc.) and can be further broken down into two subcategories: absolute method errors and relative method errors (or uncertainties).

Absolute method error refers to how well the computational results match with experimental data. Paier *et al.* calculated the mean absolute error (absolute method error), with respect to experimental values, of the G2-1 test set as 0.37 eV using VASP, with PAW potentials and the PBE ex-

change correlation functional⁴⁷ (the same as was used in the work presented here). Although the absolute method error was calculated for a large set of widely varying molecular systems (55 in total), the test set does not include any adsorbates on surface, which would be closer to the systems in the current study. Additional literature searches revealed no systematic studies of absolute method errors for adsorbates on surfaces. Although the absolute method error in this study is potentially as large as 0.37 eV, the relative method errors are expected to be much smaller.

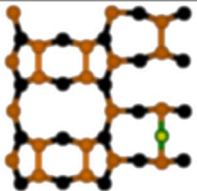
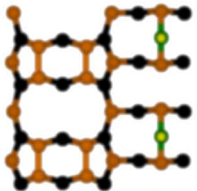
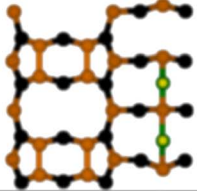
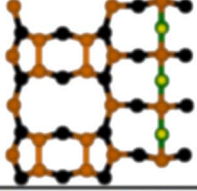
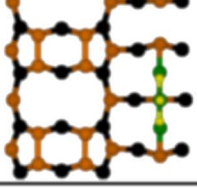
The relative method error refers to the uncertainty in the total energy difference between two similar adsorption sites. When comparing the relative total energies of a single adsorbate at two different sites on a surface, the relative error is the most important error. For example, if the relative method uncertainty is ± 0.10 eV and two structures, both having one adsorbate bonded in different locations, have adsorption energies of 1.00 and 1.05 eV then the two structures are considered to be degenerate due to computational uncertainties. A search of the literature revealed no systematic study of the relative method error for adsorbates on surfaces. However, experts in the field report differences in binding energy at similar adsorption sites on the same surface of ± 0.10 eV to be significant using computational techniques similar to the ones in the present manuscript.^{48,49} Therefore, we will assume a relative method error of ± 0.10 eV in the current study. Since the differences in calculated adsorption energy are usually much larger than ± 0.10 eV, the overall qualitative trends in both the calculations and the experiments should be in good agreement.

Both experimentally observed and nonobserved (but chemically possible) sites were modeled in an effort to verify the bonding geometries that were deduced from STM images. Tables I and II show top-down views of the calculated row and trough bonding sites, respectively, and include their corresponding enthalpies of adsorption, enthalpies of adsorption per SiO, and corrected enthalpies of adsorption per SiO (in structures that have an undimerized As atom). In order to calculate the row As dimerization energy, two clean slabs with eight row As atoms were modeled: one with the row As atoms dimerized, and the other with row As atoms undimerized. The energy difference between these two slabs amounts to four times the As dimerization energy. A similar calculation was performed to calculate the trough dimerization energy.

The DFT total energy calculations show that many of the row and trough sites are nearly energetically degenerate (Tables I and II). All of the sites that are nearly degenerate come from having two single sites in immediate proximity of each other (i.e., two SiO atoms in adjacent dimers in the $[110]$ or $[\bar{1}\bar{1}0]$ direction which are referred to as the “horizontal double” and “vertical double,” respectively). Therefore, it is only necessary to present calculations for the row and trough single sites throughout the rest of the paper.

The row/trough compact double sites were found to be less stable than the row/trough single sites by ~ 0.24 eV per SiO. In the row, the compact double site has a total corrected ΔH_{ads} of -1.74 eV (double the corrected value of -0.87 eV/SiO from Table I). The compact double site is a

TABLE II. Summary of enthalpies of adsorption for trough sites, with top-down models. The “ ΔH (total)” column displays the enthalpy of adsorption for the entire slab. The numbers in this column are divided by the number of SiO molecules per slab and the results are displayed in the “ ΔH (per SiO)” column. It is necessary to calculate the “Corrected (per SiO)” values for structures that have an undimerized surface As atom in them. To calculate the corrected values, half of the stabilization energy for an As dimer is added to the ΔH (total) value and the resulting number is then divided by the number of SiO molecules in the slab.

Trough Sites	Top Down Cut Away View	ΔH_{ads} (Total)	ΔH_{ads} (Per SiO)	Corrected (Per SiO)
Single		-1.32 eV	-1.32 eV	N/A
Vertical Double		-2.55 eV	-1.28 eV	N/A
Compact Double		-1.59 eV	-0.80 eV	-1.06 eV
Triple		-2.10 eV	-0.70 eV	N/A
Pyramid		-2.28 eV	-0.76 eV	-0.94 eV

● As ● Ga ● Si ● O

combination of a single site and an insertion site between As dimers. Since the row compact double site receives -1.08 eV of stability from the single site, it is deduced that the insertion site between As dimers only provides a -0.66 eV gain in stability. However, in the trough, the compact double site has a total corrected enthalpy of reaction of -2.12 eV; therefore, it receives an additional -0.80 eV of stabilization from the addition of the second SiO molecule between the dimers. Since the compact double site is the building block for sites that contain three SiO molecules (triple and pyramid sites), this data would imply that complexes containing three SiO molecules should be more stable in the troughs than in the rows.

Experimentally, the biggest difference in row and trough sites occurs in sites that have three SiO molecules in them (triple and pyramid sites). On the row, there are no experimentally observed sites that contain three SiO molecules, while in the trough two different sites with three SiO molecules are experimentally observed. Calculations were attempted on both the row triple and row pyramid sites. The row triple site was found to be significantly less stable than the experimentally observed row sites (single and compact double sites), and the row pyramid site was altogether computationally unstable (i.e., the pyramid consistently fell apart during geometric optimization). In contrast, the trough triple and pyramid sites were found to be stable by DFT calcula-

tions. This stabilization is attributed to the Ga atoms that protrude into the trough. An analysis of simple Coulombic potentials indicates that if the Ga atoms that protrude into the trough have as few as $\sim 0.08e^-$ in their dangling bonds, then the SiO molecules in the trough receive ~ 0.1 eV of stabilization per SiO molecule.

To determine if it is reasonable to assume that trough edge Ga atoms have a charge of $0.08e^-$, an atomic charge analysis was performed. For this analysis, the Bader method for the calculation of atomic charges was employed. In this method, the charge density minima around each atom defines where the division of charge between atoms occurs. The charge density encapsulated by these minima are then integrated to yield approximate atomic charges.⁵⁰ In order to determine the approximate number of electrons in a dangling bond on an edge Ga atom “relative” atomic charges (the difference in atomic charge between an edge Ga atom and a Ga atom in the bulk) are calculated. The relative charge was found to be $\sim 0.09e^-$. Since the number of electrons in the dangling bonds of the Ga atoms that protrude into the trough is greater than the charge needed to stabilize the trough sites by 0.1 eV per SiO, the trough sites should be expected to be more stable than the row sites.

B. Total energy versus chemical potential

The DFT adsorption energy calculations indicate that the lowest energy structures (per unit SiO) on the row and in the trough are the single sites (see Tables I and II). However, the single sites are not the most prevalent sites observed in STM images. In order to reconcile this discrepancy between theory and experiment, the SiO coverage needs to be taken into account. As the SiO coverage increases, the SiO chemical potential increases, altering the most energetically preferred adsorption geometries. A total SiO chemical potential plot was constructed using the method described by Qian *et al.*⁵¹ and normalized to the appropriate energy range.^{31,34,52} Figure 5(a) displays the lowest energy row and trough sites on one graph, clearly illustrating the fact that the trough sites are slightly more energetically preferred than the row sites. At first glance, the STM images may suggest that trough sites are not preferred over row sites; however, three of the trough sites (single, compact double, and triple sites) are not readily observed due to the previously discussed trough imaging issue, and therefore, the number of trough sites is always underestimated. Taking this into account, the experimental images are believed to verify that SiO preferentially bonds in the trough and, therefore, agree with the theoretical results in Fig. 5(a).

To study the effects of varying SiO coverage on the stability of row sites, a chemical potential plot including only row sites [Fig. 5(b)] was employed. As SiO coverage increases, the lowest energy site changes from the row single site to the row vertical double site. The row triple site maintains a significantly higher energy than the other structures and would not become the lowest energy structure until the chemical potential of SiO reaches ~ 0.8 eV. This explains why the row triple site is not observed experimentally.

The effect of SiO coverage in the trough was also ex-

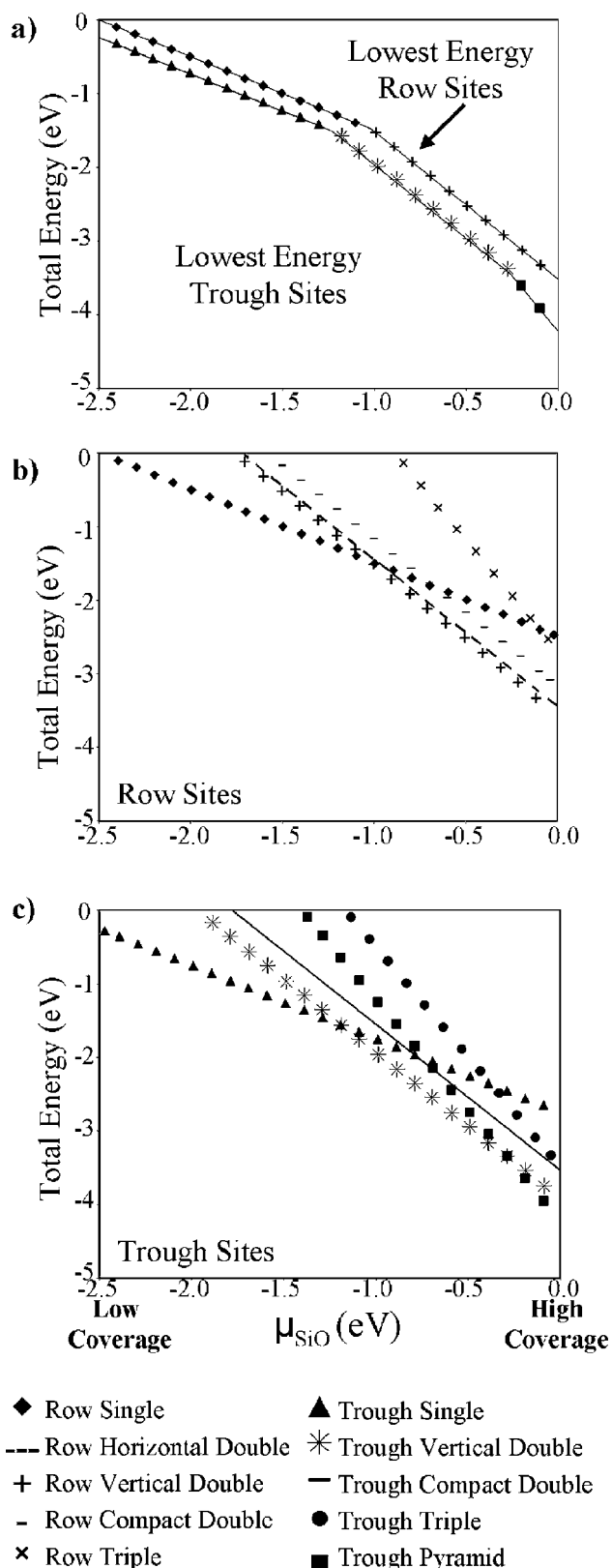


FIG. 5. The effect of SiO coverage on adsorption site stability is observed in the total energy vs chemical potential plots. As SiO coverage increases, SiO chemical potential likewise increases. (a) A plot of the most stable row and trough sites, which indicates that trough sites are slightly more stable than row sites. (b) A chemical potential plot of solely row sites, showing that the most stable row site changes from the single to the vertical double site as SiO coverage increases. (c) A chemical potential plot of solely trough sites, showing that the lowest energy site changes from the single to the vertical double and finally to the pyramid site as SiO coverage increases.

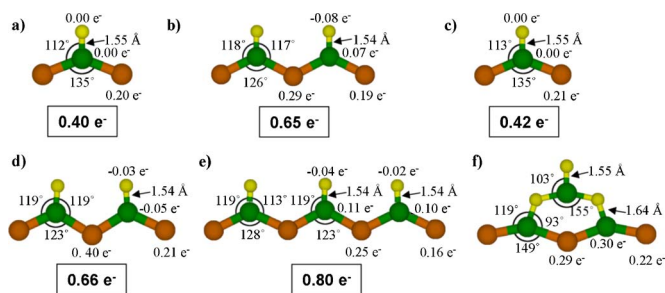


FIG. 6. The bond lengths and bond angles for each calculated SiO structures: (a) row single, (b) row compact double, (c) trough single, (d) trough compact double, (e) trough triple, and (f) trough pyramid sites. Equivalent bond angles and lengths have been averaged. In addition, relative atomic charges are displayed. The relative charges are the difference between the atomic charge on the clean surface and the surface containing the adsorbed SiO molecules. The Si and O relative charges are calculated by comparing the charge on the single sites to the charge on the Si and O atoms in the other sites. In addition the total charge buildup is boxed under each structure. Note that all of the Si atoms (except for those in the trough pyramid site) exhibit bonding angles corresponding to sp^2 hybridization. In addition, charge buildup is smaller on exterior As atoms than on interior atoms.

explored by constructing a total energy versus chemical potential plot for the trough sites [see Fig. 5(c)]. This plot reveals that the lowest energy site in the trough changes from the trough single to the trough vertical double and finally to the trough pyramid site, as the SiO coverage increases.

C. Bond angles and lengths

To verify the local charge buildup model presented in Sec. III C, the SiO bonding angles and lengths were examined for the lowest energy structures in the DFT calculations (Fig. 6). The local charge buildup model (Fig. 4) predicted that all of the Si atoms would be sp^2 hybridized except for the two Si atoms in the pyramid site that have partially filled dangling bonds, which were predicted to be sp^3 hybridized. The relaxed DFT calculated structures (Fig. 6) reveal that the Si–O bond lengths are all ~ 1.55 Å, except for the Si atoms in the pyramid site that have partially filled dangling bonds, which have Si–O bond lengths of 1.64 Å. This is consistent with what was predicted because double bonds are shorter than single bonds. In ideal sp^2 and sp^3 bonding structures, the bond angles should be 120° and 109.5° , respectively. In the structures that only contain sp^2 Si atoms [row single, row compact double, trough single, trough compact double, and trough triple Figs. 6(a)–6(e)], the bond angles (As–Si–As and As–Si–O) calculated using DFT only deviate a maximum of 15° from their ideal values. Conversely, in the trough pyramid site, all of the angles greatly deviate from the ideal angles. This suggests that the simple model of having one electron in the dangling bonds on the bottom Si atoms in the pyramid site is oversimplified and some of the charge has redistributed throughout the bonding network as well as into the dangling bond of the Si atom.

D. Scanning tunneling microscopy simulations

Tersoff-Hamann-style STM simulations⁵³ of the experimentally observed SiO adsorption sites were performed to further substantiate the assigned bonding geometries. The

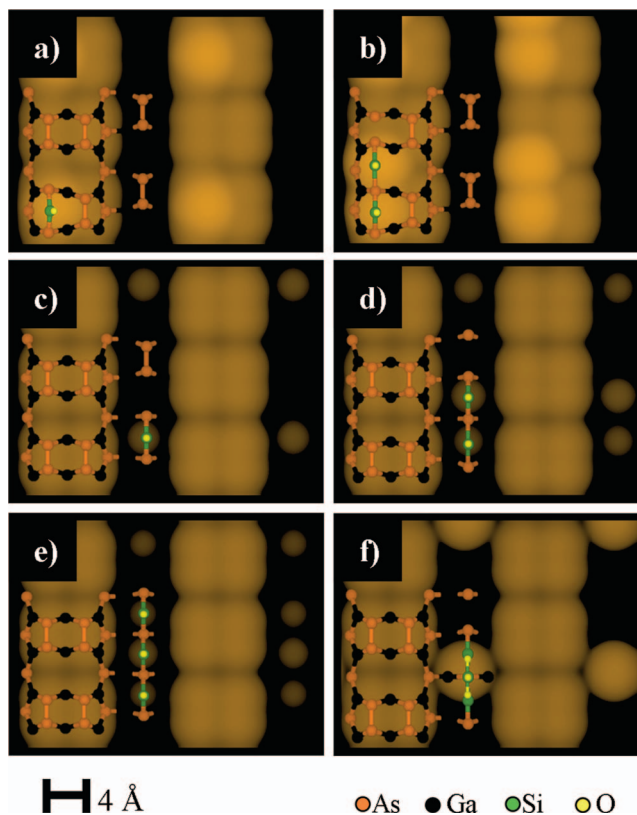


FIG. 7. (Color) STM simulations of experimentally observed sites with top-down models of the structures overlaid on the simulations: (a) row single site, (b) row compact double site, (c)trough single site, (d) trough compact double site, (e) trough triple site, and (f) trough pyramid site.

STM simulations are found in Fig. 7, including top-down views of the structures overlaid on the simulated images. The STM simulations of the row single [Fig. 7(a)], row compact double [Fig. 7(b)], and trough pyramid [Fig. 7(f)] sites are in good agreement with experiments. However, the simulated trough single [Fig. 7(c)], trough compact double [Fig. 7(d)], and trough triple [Fig. 7(e)] sites appear much higher/brighter than experimentally observed sites because these simulations do not account for the physical geometry of the tip. In experiments, the STM tip's inability to fully enter the trough causes the trough to image much more shallow than found in theoretical structural models (~ 1.5 Å versus ~ 3.0 Å deep). Therefore, any trough site (single, compact double, or triple site) that is calculated to image at 1.5 Å or below will not be directly observed in STM images but will be readily seen in STM simulations. The STM simulations, along with the total energy versus chemical potential data, confirm that the site assignments from experimental STM images are indeed correct.

E. Density of states and projected density of states

DOS and PDOS calculations were performed on the experimentally observed sites in an effort to elucidate the cause of the Fermi level pinning. These theoretical electronic structures differ slightly from the experimental (dI/dV) curves because the computational slabs are much too small for the inclusion of dopants and, therefore, are essentially intrinsic GaAs. In addition, the position of the Fermi level between

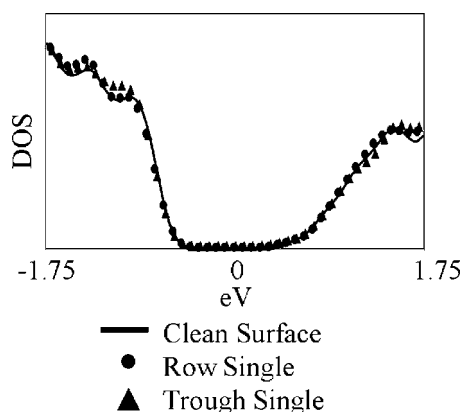


FIG. 8. DFT calculated DOS for the row single site, trough single site, and clean surface. All DOS have been normalized to 1. These simulations show that the row and trough single sites do not cause states to form within the band gap.

the valence and conduction bands is arbitrary, so for ease of comparison all the DOS and PDOS curves have been aligned at the valence bands. As a result, a modeled surface is considered unpinned if there are no states found to exist between the valence and conduction band edges.

The compact double sites and the trough pyramid site have surface As atoms that are not dimerized in the computational model (experimentally, these atoms may either remain undimerized or, if the energy barrier is low enough, they may redimerize down the row). These undimerized As atoms induce large states within the band gap region. Although the undimerized As atoms might play an indirect role in the Fermi level pinning, it is important to also explore whether the adsorbed SiO molecules themselves play a direct role in the Fermi level pinning. To negate the effects of the undimerized As atoms, H atoms were used to passivate the dangling bonds on the undimerized surface As atoms to simulate As redimerization. Once the H atoms were utilized, the states caused by the undimerized As atoms disappeared, leaving only the states directly induced by the SiO molecules. Both H atoms with a charge of 1 electron and 0.75 electrons were found to passivate the surface. The results from the calculations using one electron H atoms are presented because the electron counting model states that As atoms donate only one electron to bonds with other As atoms.³⁸

The total DOS for the row and trough single sites are given in Fig. 8. The DOS shows that no states reside in the band gap. Therefore, the single sites are expected to leave the Fermi level unpinned.

A summary of the electronic structures for the row and trough compact double sites is given in Fig. 9(a) along with a top-down view of the structures used in the calculations, Fig. 9(b) (note: with H passivation). The DOS [Fig. 9(a)] reveals that, for the compact double sites, there are no states between the valence band and conduction band edges. However, the row compact double site has a slightly narrower band gap due to conduction band edge states. Since there are no states in the band gap region the compact double sites is considered to leave the Fermi level unpinned.

A summary of the electronic structures for the trough

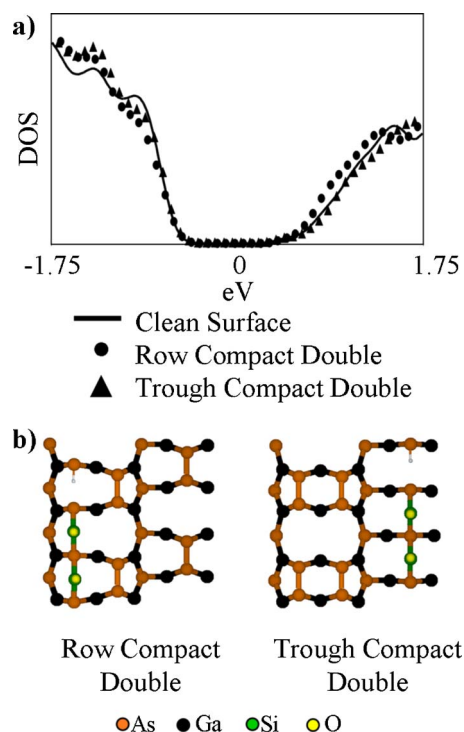


FIG. 9. (a) DOS (normalized to 1) for the row compact double site, trough compact double site, and clean surface. These simulations show that the row and trough compact double sites do not cause states to form within the band gap region. However the band gap is slightly narrower for the row compact double site. (b) Ball-and-stick diagrams of the structures used for the electronic calculation. An H atom is used to passivate the undimerized surface As atom in order to remove the states originating from the undimerized As atom.

triple site is presented in Fig. 10. The DOS for the trough triple site shows that a state resides near the conduction band edge [Fig. 10(a)]. PDOS [Figs. 10(c) and 10(d)] calculations reveal that the state generated from the trough triple site

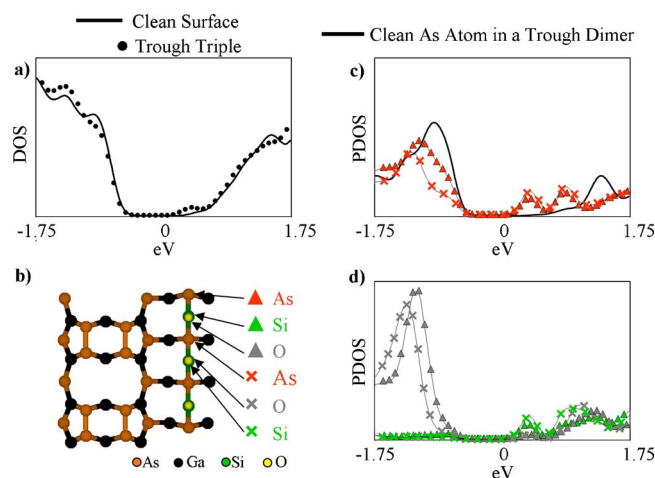


FIG. 10. (a) DOS (normalized to 1) for the clean surface and the surface containing the trough triple site. (b) Top-down model of the surface containing the trough triple site with the atoms labeled that are seen in the PDOS plots. (c) PDOS of the relevant As atoms; the PDOS of equivalent As atoms have been averaged. All PDOS have been normalized to 1. The As PDOS shows that the trough triple site causes band edge states. (d) PDOS (normalized to 1) of the Si and O atoms; the PDOS of equivalent Si and O atoms have been averaged. Similar to the As PDOS, band edge states also reside on the Si and O atoms.

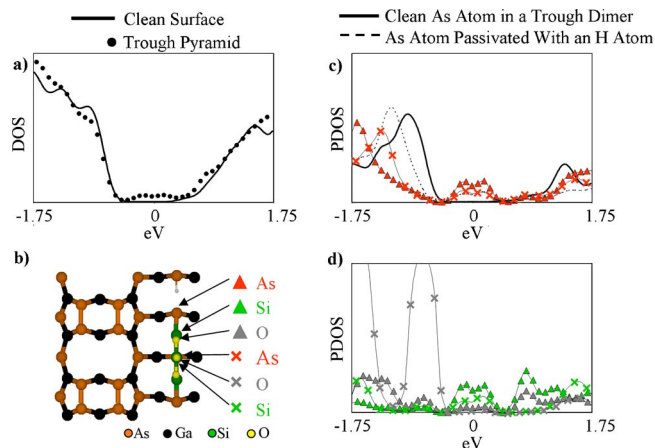


FIG. 11. (a) DOS (normalized to 1) for the clean surface and the surface containing the trough pyramid site. The undimerized As atom has been passivated with a H atom, therefore the states seen are only caused by the pyramid site. (b) Top-down model of the trough pyramid site with the atoms labeled that are seen in the PDOS. (c) PDOS (normalized to 1) of the relevant As atoms. The PDOS of equivalent As atoms have been averaged. The As PDOS shows that the trough triple site causes a state in the middle of the band gap. (d) PDOS (normalized to 1) of the Si and O atoms. The PDOS of equivalent Si and O atoms have been averaged. Similar to the As PDOS, the midgap state is also found to reside on the Si and O atoms.

resides on the surface As, Si, and O atoms. It is likely that the SiO trough triple site contributes to the experimentally observed Fermi level pinning.

Similar to the compact double site, the formation of the trough pyramid site might also result in the generation of undimerized As atoms. The electronic structure for the H-passivated trough pyramid site is presented in Fig. 11. The DOS [Fig. 11(a)] for the trough pyramid site shows that a double state resides almost in the middle of the band gap. It is possible that the two states might represent an acceptor and a donor state. The PDOS reveals [Figs. 11(c) and 11(d)] that this state extends across multiple atoms. These atoms include the SiO molecules and the As atoms in the trough; however, these states do not extend into the bulk material and are purely surface states.

F. Atomic charge analysis

An atomic charge analysis can be used to quantify the local charge buildup in these adsorption structures and explain the appearance of band gap states in the trough triple and pyramid sites. Atomic charges can be calculated using the Bader method discussed previously.⁵⁰ The relative charges are calculated from differences in atomic charges between the clean surface and a surface containing the SiO molecules (Fig. 6). In order to calculate relative charges for the Si and O atoms, the single sites were used as the standard. For row sites the row single was used as the zero point, and for trough sites the trough single was used as the zero point. The total (a sum of the surface As, Si, and O atoms) charge buildup is presented under each of the structures in Fig. 6.

Fig. 6 clearly shows that larger charge buildups occur on the interior As atoms than on exterior ones. This is consistent with what was predicted by the local charge buildup model. A subtlety that was not predicted by the local charge buildup

model is that even when no interior As atom is present [as in the case with the single sites, Fig. 6(a) and 6(c)], SiO still donates small amounts of charge to the surface As atoms; this result is understandable considering the difference in electronegativity between As and Si (2.18 vs 1.90, respectively).⁵⁴ Another assumption that the local charge buildup model made was that excess charge would preferentially migrate to the dangling bonds on the exterior As atoms. However, the atomic charge analysis revealed that the dangling bonds could only accommodate some of the extra charge, leaving large charge buildups on the interior As atoms and other Si and O atoms. Therefore, a more reliable way of quantifying the local charge buildup is by looking at the total charge buildup on all of the surface atoms (As, Si, and O).

Atomic charge analysis can be used to explain why the DOS indicated that the SiO pinned the Fermi level for some of the bonding geometries and left the Fermi level unpinned for other geometries. The DOS suggested that the Fermi level was unpinned for the row and trough single and compact double sites. Figures 6(a) and 6(c) shows that the single sites have a total charge buildup of $\sim 0.41e^-$. While the compact double sites, Figs. 6(b) and 6(c), have a total charge buildup of $\sim 0.66e^-$. The local charge buildup model predicted that there would be an increase in charge every time an additional As atom was added to the SiO bonding system. Following this logic the trough triple site would be expected to have an even larger charge buildup than the compact double sites; the Bader atomic charge analysis verifies this prediction ($0.80e^-$). Although the difference in charge buildups between the compact double and triple sites is seemingly small, it leads to a rather large charge buildup in a small region, which probably induces the band edge states seen in the DOS [Figs. 10(c) and 10(d)].

Although the trough pyramid site [Fig. 6(f)] is predicted to have a comparable charge buildup to the trough compact double site, it has an additional problem: the formation of partially filled dangling bonds on the bottom two Si atoms. This can be seen by the large relative charge of $0.34e^-$ (per Si) which resides on the bottom Si atoms in the trough pyramid site. This is consistent with Si atom having a partially filled dangling bond. As previously discussed, the Si–O bond length also indicates the presence of a single bond which would be consistent with a partially filled dangling bond on the lower Si atoms of the trough pyramid site. These partially filled dangling bonds almost certainly create the midgap states in the DOS [Fig. 11(a)].

V. CONCLUSION

Microscopic experimental techniques (STM and STS) and DFT calculations show that the exact bonding geometries of SiO on GaAs(001)- $c(2 \times 8)/(2 \times 4)$ determines the electronic structure. While some of the SiO chemisorption sites leave the Fermi level unpinned, other SiO chemisorption sites pin the Fermi level. The Fermi level pinning in the trough triple and pyramid sites was attributed to two direct causes: the buildup of charge on several consecutive As atoms and/or the formation of partially filled dangling bonds

on some of the Si atoms. In addition, some of the bonding sites (row compact double, trough compact double, and trough pyramid sites) might cause indirect pinning by generating undimerized As atoms which were shown to pin the Fermi level. The Fermi level pinning seen when SiO chemisorbs to the GaAs(001) surface is not due to the intrinsic properties of GaAs(001) and SiO but due to the specific bonding geometries at the interface.

ACKNOWLEDGMENTS

This work was funded by Motorola/Freescale Semiconductor, Inc. (97-12006) and the NSF (ITR-0315794).

- ¹G. Eftekhari, *Thin Solid Films* **257**, 110 (1995).
- ²J. L. Freeouf, D. A. Bachanan, S. L. Wright, T. N. Jackson, and B. Robinson, *Appl. Phys. Lett.* **57**, 1919 (1990).
- ³C. J. Huang, Z. S. Ya, J. H. Horng, M. P. Houng, and Y. H. Wang, *Jpn. J. Appl. Phys., Part 1* **41**, 5561 (2002).
- ⁴D. Sengupta and V. Kumar, *Phys. Status Solidi A* **73**, K279 (1982).
- ⁵H. Becke, R. Hall, and J. White, *Solid-State Electron.* **8**, 813 (1965).
- ⁶A. Colquhoun, E. Kohn, and H. L. Hartnagel, *IEEE Trans. Electron Devices* **25**, 375 (1978).
- ⁷N. Yokoyama, T. Mimura, and M. Fukuta, *IEEE Trans. Electron Devices* **27**, 1124 (1980).
- ⁸E. Kohn and A. Colquhoun, *Electron. Lett.* **13**, 73 (1977).
- ⁹R. K. Ahrenkiel and D. J. Dunlavy, *Solid-State Electron.* **27**, 485 (1984).
- ¹⁰M. Hong, M. Passlack, J. P. Mannaerts, J. Kwo, S. N. G. Chu, N. Moriya, S. Y. Hou, and V. J. Fratello, *J. Vac. Sci. Technol. B* **14**, 2297 (1996).
- ¹¹M. Passlack, M. Hong, J. P. Mannaerts, J. R. Kwo, and L. W. Tu, *Appl. Phys. Lett.* **68**, 3605 (1996).
- ¹²T. T. Chiang and W. E. Spicer, *J. Vac. Sci. Technol. A* **7**, 724 (1989).
- ¹³J. L. Freeouf and J. M. Woodall, *Appl. Phys. Lett.* **39**, 727 (1981).
- ¹⁴E. R. Weber, H. Ennen, U. Kaufmann, J. Windscheif, J. Schneider, and T. Wosinski, *J. Appl. Phys.* **53**, 6140 (1982).
- ¹⁵R. E. Allen and J. D. Dow, *J. Vac. Sci. Technol.* **19**, 383 (1981).
- ¹⁶W. E. Spicer, Z. Lilientalweber, E. Weber, N. Newman, T. Kendelewicz, R. Cao, C. McCants, P. Mahowald, K. Miyano, and I. Lindau, *J. Vac. Sci. Technol. B* **6**, 1245 (1988).
- ¹⁷M. J. Hale, J. Z. Sexton, D. L. Winn, A. C. Kummel, M. Erbudak, and M. Passlack, *J. Chem. Phys.* **120**, 5745 (2004).
- ¹⁸M. J. Hale, S. I. Yi, J. Z. Sexton, A. C. Kummel, and M. Passlack, *J. Chem. Phys.* **119**, 6719 (2003).
- ¹⁹N. Negoro, H. Fujikura, and H. Hasegawa, *Appl. Surf. Sci.* **159**, 292 (2000).
- ²⁰R. C. Blanchet and B. J. Delhomme, *Vacuum* **32**, 3 (1982).
- ²¹J. G. Tenedorio and P. A. Terzian, *IEEE Electron Device Lett.* **5**, 199 (1984).
- ²²A. Paccagnella, E. Zanoni, C. Tedesco, C. Lanzieri, and A. Cetronio, *IEEE Trans. Electron Devices* **38**, 2682 (1991).
- ²³G. J. Gerardi, F. C. Rong, E. H. Poindexter, M. Marmatz, H. Shen, and W. L. Warren, *Colloids Surf., A* **72**, 161 (1993).
- ²⁴See EPAPS Document No. E-JCPSA6-126-707641 for decapping procedure example. This document can be reached via a direct link in the online article's HTML reference section or via the EPAPS homepage (<http://www.aip.org/pubservs/epaps.html>).
- ²⁵P. Martensson and R. M. Feenstra, *Phys. Rev. B* **39**, 7744 (1989).
- ²⁶R. M. Feenstra, *Phys. Rev. B* **50**, 4561 (1994).
- ²⁷R. M. Feenstra and J. A. Stroscio, *J. Vac. Sci. Technol. B* **5**, 923 (1987).
- ²⁸J. Behrend, M. Wassermeier, L. Daweritz, and K. H. Ploog, *Surf. Sci.* **342**, 63 (1995).
- ²⁹Q. K. Xue, T. Hashizume, and T. Sakurai, *Appl. Surf. Sci.* **141**, 244 (1999).
- ³⁰J. E. Northrup and S. Froyen, *Phys. Rev. B* **50**, 2015 (1994).
- ³¹W. G. Schmidt and F. Bechstedt, *Phys. Rev. B* **54**, 16742 (1996).
- ³²T. Hashizume, Q. K. Xue, J. Zhou, A. Ichimiya, and T. Sakurai, *Phys. Rev. Lett.* **73**, 2208 (1994).
- ³³I. Chizhov, G. Lee, R. F. Willis, D. Lubyshev, and D. L. Miller, *Surf. Sci.* **419**, 1 (1998).
- ³⁴N. Moll, A. Kley, E. Pehlke, and M. Scheffler, *Phys. Rev. B* **54**, 8844 (1996).
- ³⁵V. P. LaBella, H. Yang, D. W. Bullock, P. M. Thibado, P. Kratzer, and M. Scheffler, *Phys. Rev. Lett.* **83**, 2989 (1999).
- ³⁶J. A. Stroscio, R. M. Feenstra, and A. P. Fein, *Phys. Rev. B* **36**, 7718 (1987).
- ³⁷J. A. Stroscio and R. M. Feenstra, *J. Vac. Sci. Technol. A* **6**, 577 (1988).
- ³⁸M. D. Pashley, *Phys. Rev. B* **40**, 10481 (1989).
- ³⁹G. Kresse and J. Furthmüller, *Comput. Mater. Sci.* **6**, 15 (1996).
- ⁴⁰G. Kresse and J. Furthmüller, *Phys. Rev. B* **54**, 11169 (1996).
- ⁴¹G. Kresse and J. Hafner, *Phys. Rev. B* **47**, 558 (1993).
- ⁴²G. Kresse, Technische University at Wien, 1993.
- ⁴³J. P. Perdew, K. Burke, and M. Ernzerhof, *Phys. Rev. Lett.* **77**, 3865 (1996).
- ⁴⁴P. E. Blochl, *Phys. Rev. B* **50**, 17953 (1994).
- ⁴⁵G. Kresse and D. Joubert, *Phys. Rev. B* **59**, 1758 (1999).
- ⁴⁶H. J. Monkhorst and J. D. Pack, *Phys. Rev. B* **13**, 5188 (1976).
- ⁴⁷J. Paier, R. Hirschl, M. Marsman, and G. Kresse, *J. Chem. Phys.* **122**, 234102 (2005).
- ⁴⁸N. Lorente, M. F. G. Hedouin, R. E. Palmer, and M. Persson, *Phys. Rev. B* **68**, 155401 (2003).
- ⁴⁹K. Seino, W. G. Schmidt, M. Preuss, and F. Bechstedt, *J. Phys. Chem. B* **107**, 5031 (2003).
- ⁵⁰G. Henkelman, A. Arnaldsson, and H. Jonsson, *Comput. Mater. Sci.* **36**, 354 (2006).
- ⁵¹G. X. Qian, R. M. Martin, and D. J. Chadi, *Phys. Rev. B* **38**, 7649 (1988).
- ⁵²C. G. Van de Walle and J. Neugebauer, *Phys. Rev. Lett.* **88**, 066103 (2002).
- ⁵³J. Tersoff and D. R. Hamann, *Phys. Rev. B* **31**, 805 (1985).
- ⁵⁴*Handbook of Chemistry and Physics*, 85 ed. (CRC Press, Boca Raton, 2004).